Nanoscale

Accepted Manuscript

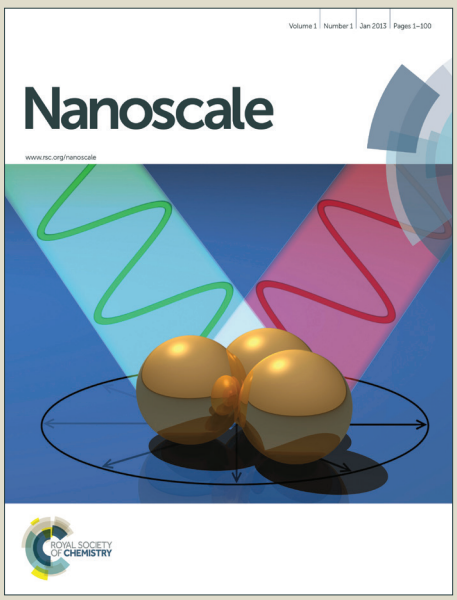

ROYAL SOCIETY OF CHEMISTRY

www.rsc.org/nanoscale

Nanoscale

ARTICLE

Si-Nanocrystal/P3HT Hybrid Film with 50- to 12-Fold Enhancement of Hole Mobility and Density: Film Prepared by Successive Drop Casting†

Received 00th January 20xx,
Accepted 00th January 20xx

DOI: 10.1039/x0xx00000x

www.rsc.org/

Daisuke Kajiya[a] and Ken-ichi Saitow*[a,b]

Hybrid silicon nanocrystal (Si-NC)/poly(3-hexylthiophene) (P3HT) films serve as the active layers of quantum dot/polymer hybrid photovoltaics. To achieve effective photovoltaic properties, it is necessary to enhance the charge carrier mobility and carrier density of the P3HT film. A 50- and 12-fold enhancement of the hole mobility and hole density, respectively, was achieved along the out-of-plane direction of a Si-NC/P3HT hybrid film, which corresponds to the carrier-migration direction between photovoltaic electrodes. According to time-of-flight, electronic absorption, Raman, atomic force microscopy, photoluminescence lifetime, and X-ray diffraction measurements, the significant enhancement of the mobility and density was attributed to both an increase in the P3HT crystallinity and the dissociation efficiency of P3HT excitons by the addition of Si-NCs to the P3HT films. These enhancements were achieved using a film preparation method developed in the present study, which has been named successive drop casting.

INTRODUCTION

Hybrid photovoltaics composed of both organic polymers and inorganic nanomaterials have attracted much attention in the field of material science for industrial applications, due to advantages in both the ease of organic polymer solution processing and the stability of inorganic materials.[1–3] The power conversion efficiency of the hybrid photovoltaic has exceeded 5% for $PbS_{0.4}Se_{0.6}$-nanocrystals/polymer and that of organic polymer photovoltaics has reached 10% (Table S1†). The poly(3-hexylthiophene) (P3HT) polymer has been the most popular material for hybrid photovoltaics[4–8] in conjunction with Si,[9–20] Ge,[21] GaAs,[22] CdS,[23,24] CdSe,[25–27] Bi_2S_3,[28] TiO_2,[29–32] ZnO,[33–37] Cu_2S,[38] or $CuInS_2$[39] nanomaterials as inorganic semiconductors (Table S1†). In particular, Si nanomaterials have attracted much attention due to the natural abundance of Si, which is environmentally benign and exhibits efficient multi-exciton generation.[40–42] Thus, Si/P3HT hybrid photovoltaics have been investigated by various research groups using Si nanocrystals,[9–13] nanorods,[14] nanopillars,[15,16] nanowires,[17–19] nanoholes,[19] and thin film layers.[20] The power conversion efficiency was recently reported to be greater than 10% for a hybrid photovoltaic composed of P3HT and Si nanoholes fabricated on a Si wafer.[19] However, the carrier mobility is also a crucial parameter for enhancing the performance of hybrid photovoltaics.[43,44] An increase in the mobility in hybrid films compared with that in pristine film was reported for systems such as CdSe/P3HT,[26,27] CdS/P3HT,[24] and TiO_2/P3HT,[29,31,32] whereas a decrease in mobility was observed in Si/P3HT[9] and ZnO/P3HT[37] films. In order to realize high-performance hybrid photovoltaics, in addition to evaluating the carrier transport properties, it is important to study the film morphology and structure, including the presence of nanoscale interfaces. Different film preparation methods also need to be investigated.

We have fabricated photofunctional nanomaterials by pulsed laser ablation (PLA).[45–52] In the present study, Si nanocrystals (Si-NCs) prepared by PLA of a Si wafer in 2-propanol were used to fabricate a Si/P3HT hybrid film (Fig. 1a). The film was produced using a newly developed method referred to as "successive drop casting", which is an improvement on the conventional drop casting technique. The hole mobility and hole density were measured using a time-of-flight (TOF) technique. Electronic absorption spectroscopy, Raman spectroscopy, atomic force microscopy (AFM), photoluminescence (PL) lifetime, and X-ray diffraction (XRD) measurements were conducted in order to examine the effect of Si-NCs addition to P3HT. The results for the Si/P3HT hybrid system were compared with those for a pristine P3HT film prepared using the same procedure, except for the addition of Si-NCs. It was found that the presence of Si-NCs led to 50- to 12-fold improvement in the hole transport properties. The successive drop casting method produced a Si/P3HT hybrid film with a high degree of crystallinity, a good morphology, and a homogeneous structure, which led to a high hole mobility and efficient dissociation of P3HT excitons.

[a] Natural Science Center for Basic Research and Development (N-BARD), Hiroshima University, 1-3-1 Kagamiyama, Higashi-hiroshima, Hiroshima 739-8526, Japan
[b] Department of Chemistry, Graduate School of Science, Hiroshima University, 1-3-1 Kagamiyama, Higashi-hiroshima, Hiroshima 739-8526, Japan
† Electronic Supplementary Information (ESI) available. See
DOI: 10.1039/x0xx00000x

Experimental

Preparation of Si-NCs

Si-NCs were generated by PLA of a Si wafer (Nilaco, 500441) immersed in 2-propanol. The light source used for PLA was the second harmonic of a Nd:YAG laser (Rayture Systems, RH-30) operated at an excitation wavelength of 532 nm, a pulse width of 7 ns, an energy of 19 mJ/pulse, and a repetition rate of 20 Hz. The average size of the Si-NCs produced was 8 nm, which was determined from dynamic light scattering (DLS) measurements. Raman spectroscopy measurements revealed that the Si products were not amorphous, but crystalline (Fig. S1†). As for the study on the size dependence, the Si-NCs were prepared from 5 nm to 14 nm by changing the PLA condition (Fig. S2†).

Film Preparation

All processes except for deposition of the Al cathode were conducted in air. The Si-NC/P3HT hybrid film was prepared by successive drop casting of two solutions: Si-NCs dissolved in 2-propanol at a concentration of 0.25 mg/mL were first dropped onto a pre-cleaned ITO-coated glass substrate at 60 °C, followed by the drop casting of P3HT dissolved in chlorobenzene onto the Si-NCs at room temperature before drying. The weight ratio of the solvents on the ITO-coated glass substrate was 2 wt% 2-propanol and 98 wt% chlorobenzene, which was determined using an analytical balance (Sartorius, MC1). The Si-NC and P3HT solutions were stirred on the substrate for 20 s, and the film was then dried for 12 h at room temperature. This process produced a hybrid film with improved morphology and a smoother surface than that formed using a drop cast mixed solution of Si-NCs and P3HT, as determined from optical and laser microscope observations. The solvent effect on the film morphology and carrier migration processes were also investigated for the successive drop casting process, as described in Note S1†. Electronic grade P3HT (regioregularity 91–94%, molecular weight M_w = 50,000–70,000, item # 4002-E, Rieke Metals) was used and the concentration of Si-NCs in the hybrid film was determined gravimetrically with an analytical balance. A 4-mm-diameter and 100-nm-thick Al cathode film was deposited on the hybrid film using a vacuum evaporation system (Sanyu Electron, SVC-700TM). After deposition of the Al cathode, thermal annealing was conducted on a hot plate (Barnstead Thermolyne, Cimarec) at 120 °C for 30 min.

All procedures for the preparation of the pristine film were the same to those used for the hybrid film, except for the addition of Si-NCs. The pristine P3HT film was prepared by drop casting a solution of P3HT in chlorobenzene onto ITO-coated glass at room temperature in air. The film was dried for 12 h at room temperature in air. An Al cathode was then deposited and the film was annealed at 120 °C for 30 min in air. The thicknesses of the pristine P3HT and hybrid films were measured using a confocal laser microscope (Shimadzu, OLS4000) equipped with a 100× objective; the thicknesses ranged from 5 to 13 μm with a standard deviation of 0.5 μm.

TOF Measurements

An in-house-built instrument was used for TOF measurements.[53] The light source was the second harmonic of a Nd:YAG laser (λ = 532 nm, 7 ns, and 6 Hz). The pulsed energy was carefully adjusted to 0.5 μJ/pulse using an attenuator and a laser energy sensor (Coherent, J-10MB-LE). A silicon PIN photodiode (Electro-Optics Technology, ET-2030) was used to provide a trigger pulse. The sample film was irradiated by the pulsed laser from the ITO anode side. The generated holes were transferred to the Al cathode by the applied voltage. Transient time profiles of the hole dynamics, as a positive-voltage signal, were stored in a digital oscilloscope (Tektronix TDS3054) for 512 accumulations. All TOF signals were carefully collected using the sample enclosed in an aluminum alloy Faraday cage to minimize electrical noise and also obtained at the condition of geometrical charge >> collected charge, as described in Note S2†. The TOF measurements were also conducted at the condition of a sheet-like carrier formation, corresponding to an intersection character between a plateau and a tail. It was confirmed that the holes do not transport through only Si-NCs, according to the measurements of concentration dependence of Si-NCs in the film (Note S3†). The load resistance for was set to 50 Ω to determine the accurate transit time with a high time resolution, and was set to 1 kΩ to detect a clear TOF signal for the hole density evaluation.

PL Decay, Absorption, AFM, Raman, SEM/EDS, DLS and FTIR Measurements

PL decay was measured using a time-to-amplitude converter (TAC), based on a photon counting method (Horiba Jobin Yvon, FluoroCube) and a diode laser at an excitation wavelength of 453 nm and a luminescence wavelength of 720 nm. Transmission spectra were measured for a sample (film on ITO glass substrate), reference (ITO glass substrate), and dark signals using a deuterium-halogen lamp (Ocean Optics, USB-DT) and a multichannel CCD detector (Ocean Optics, USB4000). Absorption spectra of the pristine P3HT and hybrid films were obtained on the basis of the Beer-Lambert law. AFM height images were obtained in tapping mode using a microscope (Shimadzu, SPM-9700) equipped with a microcantilever (Olympus, OMCL-AC200TS-C3) with a spring constant of 9 N/m and a resonance frequency of 150 kHz. Raman spectra were measured using a Raman microscope (Horiba Jobin Yvon, LabRam HR800) with a backscattering geometry and a 100× objective, a 1800 line/mm grating, and a CCD camera. An Ar^+ laser (Melles Griot, 543-AP-A01) was used at an excitation wavelength of 488 nm as the light source for the Raman spectral measurements of films and the laser power was set to 0.5 μW at the film surface. Elemental mapping of the hybrid film cross-section was measured using an SEM (Hitachi High-Technologies, S-5200) operated at an acceleration voltage of 10 kV and equipped with an EDS system (EDAX, Genesis XM2). DLS measurements of Si-NCs dispersed in 2-propanol were performed using a particle size analyzer (Malvern Instruments

Ltd., Zetasizer Nano ZS) at a laser wavelength of 532 nm. Fourier transform infrared (FTIR; Jasco, FT/IR-4200) spectroscopy of Si-NCs was conducted using the attenuated total reflectance (ATR) method. Spectra were measured for droplets of sample (Si-NCs in 2-propanol) and reference (2-propanol) on an ATR prism made of ZnSe (ATR PRO450-S, Jasco).

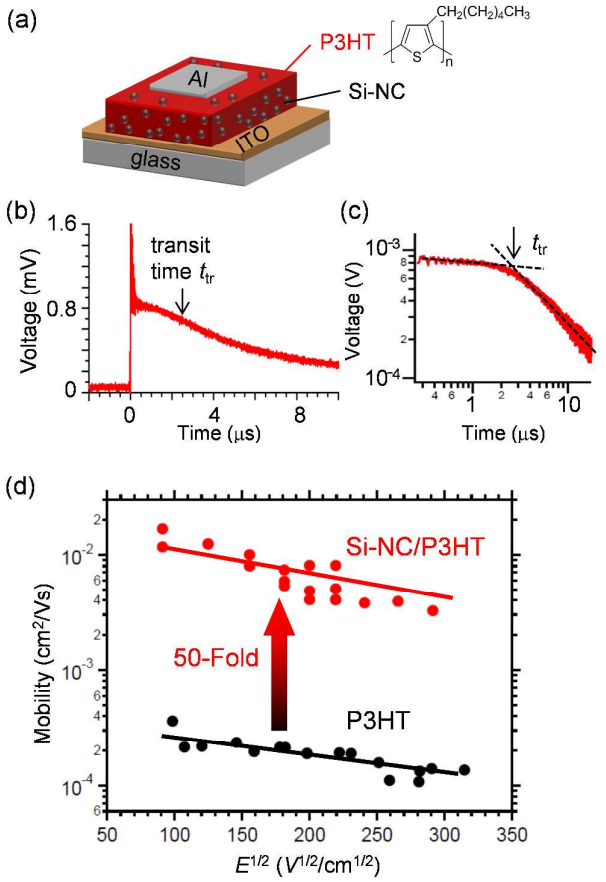

Fig. 1. (a) Schematic illustration of the Si-NC/P3HT hybrid film. (b) A typical TOF signal for holes in P3HT measured by excitation of the hybrid film. The pulsed energy, film thickness, electric field, and load resistance were 0.5 μJ/pulse, 10 μm, 220 $V^{1/2}/cm^{1/2}$, and 50 Ω, respectively. The Si-NCs size and concentration are 8 nm and 25wt%, respectively. (c) Double-logarithmic plot of Fig. 1b, where dashed lines represent the crossing point to obtain the transit time. (d) Hole mobilities for the Si-NC (25wt%, 8 nm)/P3HT hybrid and pristine P3HT films as a function of the electric field.

Results and discussion

Fig. 1b shows a typical TOF signal for holes in the Si-NC/P3HT hybrid film generated by pulse laser irradiation at an excitation wavelength of 532 nm, at which the absorbance of P3HT is 150 times greater than that of Si-NCs (Fig. S3†). The signal magnitude corresponds to the time-dependent photocurrent.[54] The time profile is composed of a fast rise, a successive fast decay, a plateau, and a slow decay. The fast rise and decay components are assigned to the generation and disappearance of holes, respectively, due to photoabsorption and recombination immediately after laser irradiation. Their time scales are instantaneous within pulse width and tens of nanoseconds, respectively. The disappearance of hole represents the recombination between hole and electron (Fig. S4†). The plateau is confirmed by the double-logarithmic plot of the time profile, as shown in Fig. 1c, and is assigned to the hole transport process in the hybrid film. The slow (second) decay is due to the dispersion of hole transport and/or trapping in the inhomogeneous hybrid film and its time scale is tens of microseconds.[55,56] To obtain the hole mobility, the transit time (t_{tr}) is determined from the intersection between the plateau and the slow decay components,[55,56] as shown in Fig. 1c. The hole mobility (μ) is calculated using the equation $\mu = d/Et_{tr}$,[55,56] where d is the film thickness and E is the electric field applied to the film. Fig. 1d shows the hole mobilities for a Si-NC/P3HT hybrid film and a pristine P3HT film as a function of E. The hole mobility for the pristine P3HT film is $(2.0\pm0.2)\times10^{-4}$ $cm^2/(V\cdot s)$,[57,58] which is almost equivalent to that previously reported[5,56,59,60] (Fig. S5†). In contrast, the addition of Si-NCs to P3HT to form the hybrid film causes a 50-fold enhancement of the hole mobility to $(9.7\pm1.1)\times10^{-3}$ $cm^2/(V\cdot s)$ (Fig. 1d).[57,58]

Figs. 2a and 2b show AFM images of the pristine P3HT and Si-NC/P3HT hybrid films, respectively. The brightness in the images indicates the height from the film surface. Many P3HT nanowires with lengths of ca. 1 μm and diameters of ca. 20 nm are evident in the hybrid film, whereas no nanowires are present in the pristine P3HT film. It has been elucidated that the P3HT nanowires are composed of highly ordered monomers due to π–π stacking interaction[23,61–64] (Fig. 2b, inset). Highly ordered P3HT monomers generate local increases in P3HT crystallinity in the hybrid film. Figs. 2c and 2d show P3HT electronic absorption spectra (π-π* transition) for the pristine P3HT and Si-NC/P3HT hybrid films, respectively. The spectral features in the lower and higher energy regions have been attributed to aggregated and unaggregated components, respectively.[65,66] It can be seen that the integrated intensity of the aggregated spectral component is larger in the hybrid film, while that of the unaggregated spectral component is smaller. To confirm these results, vibrational Raman spectroscopy was carried out, and the spectra for the pristine and hybrid films are shown in Figs. 2e and 2f, respectively. The bands around 1450 and 1470 cm^{-1} are assigned to the C=C stretching modes of aggregated and unaggregated components, respectively.[67–70] Again, the integrated intensity of the aggregated spectral component is larger in the hybrid film.[71] In addition, the increase of P3HT crystallinity was confirmed in the hybrid film (Fig. S6†), according to the result of XRD measurements. Consequently, the experimental results from AFM, electronic absorption spectroscopy, vibrational Raman spectroscopy, and XRD indicate that the addition of Si-NCs to P3HT increases the crystallinity and aggregation of P3HT monomers.

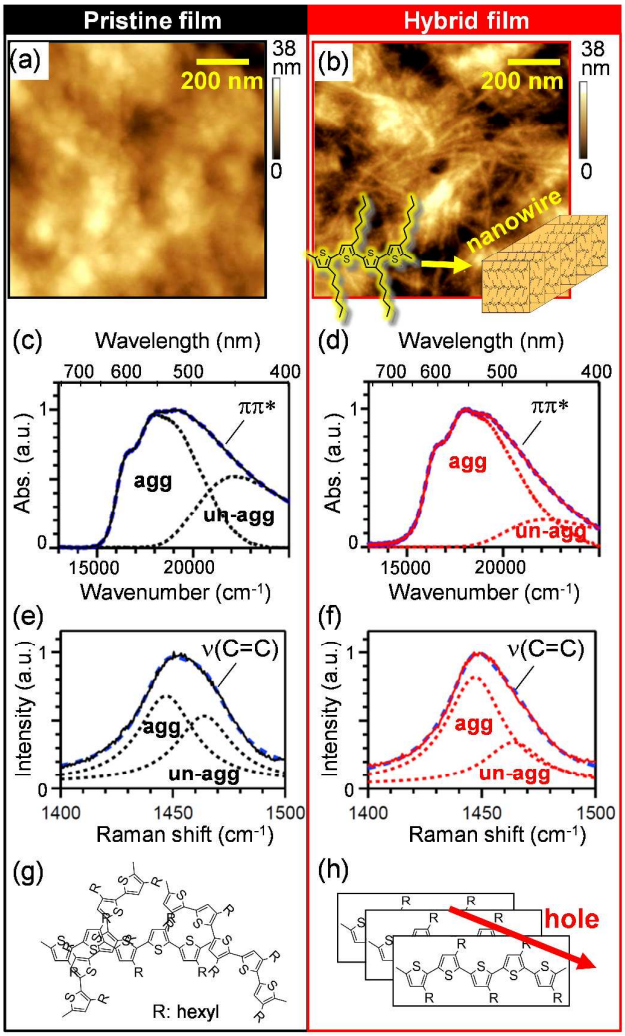

Fig. 2. Data used to characterize the morphologies and structures of pristine P3HT and Si-NC/P3HT hybrid films. The Si-NCs size and concentration of the hybrid film are 8 nm and 25wt%, respectively. (a,b) AFM height images. (c,d) Absorption spectra divided into aggregated (agg) and unaggregated (un-agg) bands. Blue dotted lines are the sum of agg and un-agg bands. (e,f) Raman spectra of C=C stretching modes of P3HT measured with an excitation wavelength of 488 nm. (g,h) Schematic diagrams of P3HT chains.

Another notable result in the present study is the magnitude of the TOF signal (Fig. 3a): the integrated intensity of the TOF signal can give the hole density generated in the film (see Note S4†). Thus, it was elucidated that the hole density in the hybrid films is 12 times that in the pristine P3HT film. This result indicates that the hole density is increased by the addition of Si-NCs to P3HT. The PL decay for P3HT was measured to investigate the mechanism for the increase in hole density. Fig. 3b shows time profiles for the PL of pristine P3HT and Si-NC/P3HT hybrid films measured at an excitation wavelength of 453 nm and a luminescence wavelength of 720 nm. The PL intensity for the hybrid film decayed faster than that for the pristine P3HT film, which indicates the rapid dissociation of P3HT excitons by the addition of Si-NCs to P3HT: the PL-decay time is sub-nanosecond and is 100 times faster than that of the TOF-decay (tens of nanoseconds). To confirm the faster dissociation of excitons in the hybrid film, the film structure was investigated by Si elemental mapping using scanning electron microscopy/energy-dispersive X-ray spectroscopy (SEM/EDS). Fig. 4 shows that the Si-NCs are distributed homogeneously throughout the hybrid film; therefore, a large amount of heterointerfaces exist between the Si-NCs and P3HT. A heterostructure with a large total interface area is effective for the dissociation of P3HT excitons into holes and electrons. The electrons associated with P3HT excitons can be transferred to the conduction band of the Si-NCs,[67] while the holes remain, as illustrated schematically in Fig. 3c. In fact, the PL lifetime is reduced by increasing the Si-NCs concentration, according to the results of Si-NCs concentration dependence (Fig. S7†). Consequently, the P3HT excitons decay faster with increasing heterointerface area, as shown in Fig. 3b, and faster dissociation results in an increase in the hole density, as shown in Fig. 3a.

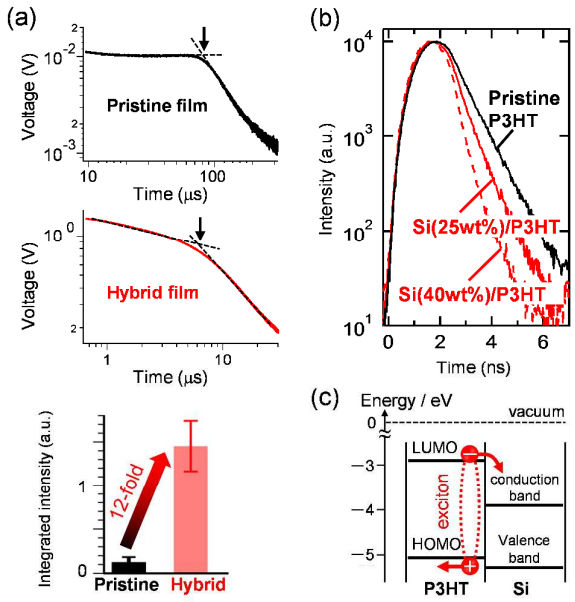

Fig. 3. (a) Double-logarithmic plots of TOF signals for pristine P3HT film (top) and Si-NC(8nm size, 25wt%)/P3HT hybrid film (middle), measured at a pulsed energy of 0.5 μJ/pulse, d = 6 μm, $E^{1/2}$ = 290 $V^{1/2}/cm^{1/2}$, and a load resistance of 1 kΩ. Dashed lines indicate asymptotes to the plateau and declining slopes, and arrows indicate the transit times. The lower panel shows the integrated intensities of the TOF signals for both films. The error bar represents the standard deviation for 5 measurements. The calculation method is described in Note S4†. (b) PL decay for pristine P3HT, hybrid Si-NC (8nm size, 25 wt%)/P3HT, and Si-NC (8nm size, 40 wt%)/P3HT films at excitation and luminescence wavelengths of 453 and 720 nm, respectively. (c) Schematic illustration of P3HT exciton dissociation. The band diagram is reproduced from Fig. 1 of Ref. 72. The LUMO level of P3HT lies above the conduction band of Si, which enables exciton dissociation and electron transfer to Si.

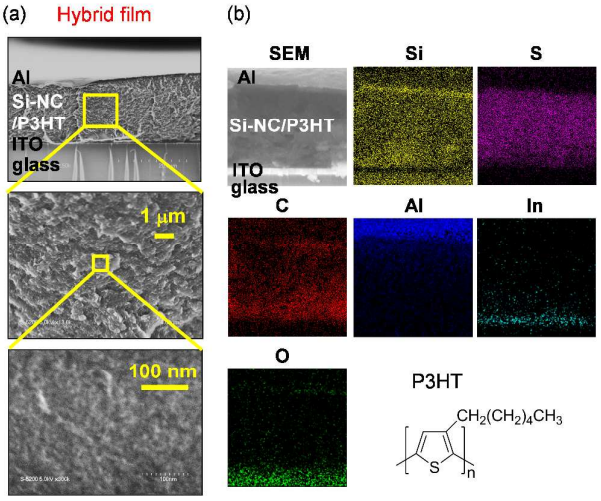

Fig. 4. (a) Cross-sectional SEM images of Si-NC(25wt%, 8nm size)/P3HT hybrid film and (b) EDS elemental maps for silicon, sulfur, carbon, aluminum, indium, and oxygen.

The enhancement of the hole mobility and hole density along the out-of-plane direction of the Si-NC/P3HT hybrid film was 50-fold and 12-fold, respectively. These enhancements are achieved by the developed film-preparation method, i.e., successive drop casting. Fig. 5a shows a schematic diagram of the successive drop casting technique, which involves drop casting a Si-NC solution followed by drop casting the P3HT solution onto an indium tin oxide (ITO)-coated glass substrate. The two solutions are gently blended on the substrate, which provides the film with a good morphology and a smooth surface, as shown Fig. 5b. In contrast, conventional drop casting does not produce a film with good morphology and a smooth surface at the same film thickness, as shown in Fig. 5b. Namely, the blending of the two solutions on the substrate is important, because gentle blending can suppress the heterogeneous nucleation that causes nanoparticle aggregation in solution, while intense mixing promotes particle aggregation in the solution.[73,74] In fact, the roughness of the film prepared by successive drop casting is 9 times smaller than that prepared by conventional drop casting under the condition of the same film thickness, as shown in Fig. 5b. AFM measurements showed that the P3HT nanowires are produced by the successive drop casting and are not produced by the conventional drop casting, as shown in Fig. 6a. This result indicates that the conventional drop casting provides the highly ordered P3HT monomers. Raman spectroscopic measurements also showed that the successive drop casting increases P3HT aggregations, which are established by many P3HT-monomer molecules with a planar backbone structure, as shown in Fig. 6b. Namely, the lower-energy component of the Raman spectrum in the film prepared by the successive drop casting is larger than that in the film prepared by the conventional drop casting.[66] In addition, for a critical checking, we investigated whether the solvent used in the Si-NC solution affected the film morphology and mobility; however, it was determined that there was no influence of the solvent (see Note S1†).

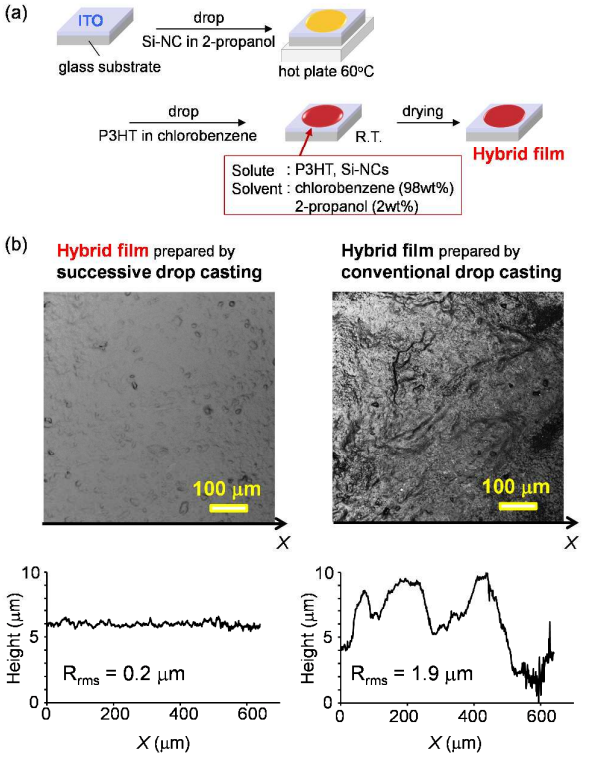

Fig. 5. (a) Schematic diagram of the successive drop casting method (details in Experimental section) for the preparation of the hybrid film. (b) Morphologies of the Si-NC(8nm, 25wt%)/P3HT hybrid films prepared by successive drop casting (left) and conventional drop casting (right). Laser microscope images (top) and their surface roughness (bottom). R_{rms} represents the root-mean-squared surface roughness. Both the films are prepared at the same film thickness (d = 6 μm).

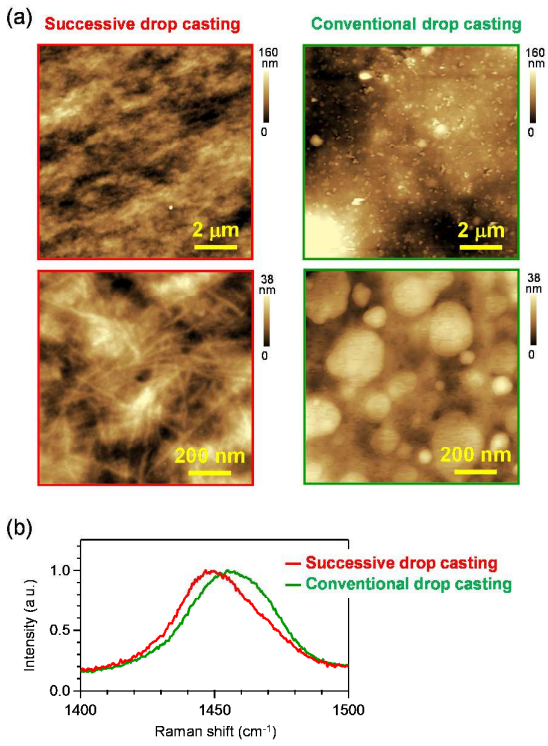

Fig. 6. (a) AFM height images of Si-NC(8nm, 25wt%)/P3HT hybrid films prepared by successive drop casting and conventional drop casting. (b) Raman spectra of the C=C stretching modes of P3HT of the Si-NC/P3HT hybrid films, measured at an excitation wavelength of 488 nm. The film thickness is 6 μm.

To further confirm the validity of the successive drop casting, we measured the hole mobilities and densities of hybrid films by changing the Si-NCs size, Si-NCs concentration, and film thickness, as shown in Fig. 7. The results show that the hole mobilities and densities of all the hybrid films are greater than those of the pristine film. Thus, it was ensured that the successive drop casting is a general method for the current system.

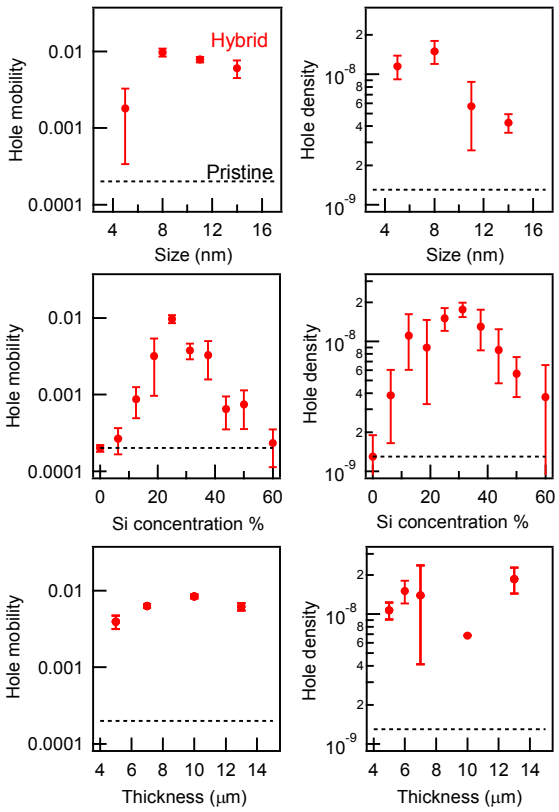

Fig. 7. Hole mobilities (cm^2/Vs) and densities (C) as functions of Si-NC size (top), Si-NC concentration in the film (middle), and film thickness (bottom). Dot line is the values of the hole mobility and density for the pristine film. Si-NCs with different size are prepared by PLA method (Fig. S2†). The data of Si concentration and thickness dependences are measured using Si-NCs with the size of 8 nm.

The hole mobility for the Si-NC/P3HT hybrid film obtained in the present study is discussed with respect to that previously reported.[9] The present study shows an increase in P3HT hole mobility in the hybrid film, as shown in Fig. 1, whereas the previous study reported a decrease in hole mobility by the addition of Si-NCs to a P3HT film.[9] The P3HT used in both studies had the same regioregularity (RR = 91–94%) and molecular weight (M_w = 50–70 K)[75], and the same direction of carrier migration was used for the mobility measurements. However, there are several differences between the two studies, the details of which are listed in Table S2†. Five specific factors were discussed. 1) Successive drop casting was used in the present study, whereas spin-coating was used in the previous study. Successive drop casting provides the hybrid film with a good morphology, a higher degree of aggregation, a smooth surface, a homogeneous distribution of Si-NCs, and a higher degree of crystallinity. In fact, the absorption and Raman results at the same film thickness give that the film prepared by the successive drop casting shows more aggregates and higher planarity than the film prepared by the spin coating (Fig. S8†). 2) The film thicknesses in the present and previous studies were 5–13 μm and 150 nm, respectively, and the thicker film requires a slower and/or longer drying time, which produces a highly ordered P3HT thin film.[76–79] 3) There is a difference between annealing conditions employed, which influence the morphology of the P3HT film,[9,76,80,81] i.e., 120 °C at 30 min in the present study and 150 °C at 120 min in the previous study. 4) As for the size of Si-NC and the concertation of Si-NC in the hybrid film, their ranges in the present study involve the size and concentration in the previous study, but the mobility in the present study shows higher than that of the previous study in the all particle size and all concentrations. 5) The Si-NCs used in the present study were synthesized by pulsed laser ablation in the liquid phase, while those in the previous study were prepared by plasma synthesis in a vacuum. The present Si-NCs are terminated by H, CH_x, and SiO_x according to the IR spectroscopy measurements (Fig. 9),[82] while the Si-NCs in the previous study are terminated by H. The difference of Si surface is important for the P3HT morphology, that is, the π–π stacking of P3HT is ordered by the π–H interaction at the Si surface passivated with CH_x group, based on results of XRD and transmission electron microscopy (TEM).[86,87] The current result of XRD also shows that the addition of Si-NCs increases P3HT crystallinity (Fig. S6†).

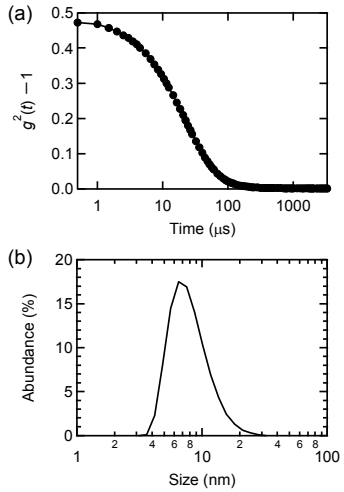

Fig. 8. Typical DLS result of Si-NCs of 8 nm average size. (a) Time-correlation function of Si-NCs measured by DLS. (b) Size distribution of Si-NCs obtained from the correlation function.

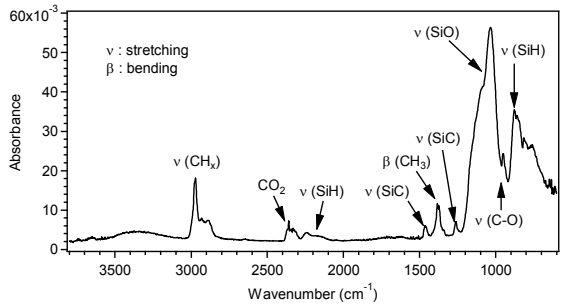

Fig. 9. FTIR spectrum of 8 nm Si-NCs prepared by PLA. The Si–C stretching modes are observed at around 1250 and 1460 cm^{-1}, and the C–H_x related modes are observed at around 3000 and 1380 cm^{-1}.[52] The bands at around 1100 cm^{-1} are assigned to Si–O related vibration modes,[52] and the peaks around 2100 and 900 cm^{-1} are assigned to Si–H related vibration modes.[9] The peak around 950 cm^{-1} is assigned to the C–O stretching mode.[85]

Conclusions

A Si-NC/P3HT hybrid film and a pristine P3HT film were prepared using successive drop casting and were evaluated using TOF, electronic absorption spectroscopy, Raman spectroscopy, AFM, lifetime, SEM/EDS, and XRD measurements. The hole mobility and density along the out-of-plane direction (carrier migration direction in a photovoltaic) of the Si-NC/P3HT hybrid film were enhanced 50- and 12-fold, respectively, with respect to the pristine P3HT film. The enhancement of hole mobility is attributed to the increase in P3HT crystallinity in the hybrid film, based on electronic absorption spectroscopy, Raman spectroscopy, AFM, and XRD observations. The enhancement of the hole density is attributed to an increase in the dissociation of P3HT excitons in the hybrid film, based on PL lifetime and SEM/EDS measurements. The successive drop casting preparation method developed in the present study was a crucial factor in the enhancement of both the hole mobility and density in the Si-NC/P3HT hybrid film. This method produces a hybrid film with a good morphology, a smooth surface, and a homogeneous distribution of inorganic nanocrystals in the organic polymer via a solution process. In addition, the hybrid film in conjugation with the Si-NCs has a high degree of crystallinity due to the surface structure of Si-NCs produced by PLA in a liquid. These results will provide an important contribution to enhancing the optoelectronic performance of hybrid films in the out-of-plane direction for the development of quantum dot/polymer hybrid photovoltaics.

Acknowledgements

The authors acknowledge Prof. Ryuzi Katoh of Nihon University for advices on the construction of TOF instrument and the TOF measurements. This work was supported by the Funding Program for the Next Generation World-Leading Researchers (GR073) of the Japan Society for the Promotion of Science (JSPS).

Notes and references

1 W. U. Huynh, J. J. Dittmer and A. P.Alivisatos, *Science*, 2002, **295**, 2425–2427.
2 J. Weickert, R. B. Dunbar, H. C. Hesse, W. Wiedemann and L. Schmidt-Mende, *Adv. Mater.*, 2011, **23**, 1810–1828.
3 K. M. Coakley and M. D. McGehee, *Chem. Mater.*, 2004, **16**, 4533–4542.
4 B. C. Thompson and J. M. J. Fréchet, *Angew. Chem. Int. Ed.*, 2008, **47**, 58–77.
5 R. Mauer, M. Kastler and F. Laquai, *Adv. Funct. Mater.*, 2010, **20**, 2085–2092.
6 S. S. Li and C. W. Chen, *J. Mater. Chem. A*, 2013, **1**, 10574–10591.
7 S. Ren, M. Bernardi, R. R. Lunt, V. Bulovic, J. C. Grossman and S. Gradecak, *Nano Lett.*, 2011, **11**, 5316–5321.
8 B. Paci, G. D. Spyropoulos, A. Generosi, D. Bailo, V. R. Albertini, E. Stratakis and E. Kymakis, *Adv. Funct. Mater.*, 2011, **21**, 3573–3582.
9 C. Y. Liu, Z. C. Holman and U. R. Kortshagen, *Adv. Funct. Mater.*, 2010, **20**, 2157–2164.
10 V. Svrcek, *Optoelectronic Devices and Properties*; Sergiyenko, O., Ed., InTech, 2011, Chapter 10.
11 R. Dietmueller, A. R. Stegner, R. Lechner, S. Niesar, R. N. Pereira, M. S. Brandt, A. Ebbers, M. Trocha, H. Wiggers and M. Stutzmann, *Appl. Phys. Lett.*, 2009, **94**, 113301-1–113301-3.
12 Y. Ding, R. Gresback, R. Yamada, K. Okazaki and T. Nozaki, *Jpn. J. Appl. Phys.*, 2013, **52**, 11NM04-1–11NM04-5.
13 Y. Ding, R. Gresback, Q. Liu, S. Zhou, X. Pi and T. Nozaki, *Nano Energy*, 2014, **9**, 25–31.
14 W. Guo, F. Liu, M. Zhu, Y. Zhou and J. Liu, *Phys. Status Solidi C*, 2011, **8**, 2810–2813.
15 V. Gowrishankar, S. R. Scully, A. T. Chan, M. D. McGehee, Q. Wang and H. M. Branz, *J. Appl. Phys.*, 2008, **103**, 064511-1–064511-8.
16 F. Zhang, X. Han, S. Lee and B. Sun, *J. Mater. Chem.*, 2012, **22**, 5362–5368.
17 X. Lei, F. Zhang, T. Song and B. Sun, *Appl. Phys. Lett.*, 2011, **99**, 233305-1–233305-3.
18 S. Tsai, H. Chang, H. Wang, S. Chen, C. Lin, S. Chen, Y. Chueh and Jr-H. He, *ACS Nano*, 2011, **5**, 9501–9510.
19 Y. Wu, X. Zhang, J. Jie, C. Xie, X. Zhang, B. Sun, Y. Wang and P. Gao, *J. Phys. Chem. C*, 2013, **117**, 11968–11976.
20 P. J. Alet, S. Palacin, P. R. I. Cabarrocas, B. Kalache, M. Firon and R. Bettignies, *Eur. Phys. J. Appl. Phys.*, 2007, **36**, 231–234.
21 B. Sun, G. Zou, X. Shen and X. Zhang, *Appl. Phys. Lett.*, 2009, **94**, 233504-1–233504-3.
22 S. Ren, N. Zhao, S. C. Crawford, M. Tambe, V. Bulovic and S. Gradecak, *Nano Lett.*, 2011, **11**, 408–413.
23 S. Ren, L. Y. Chang, S. K. Lim, J. Zhao, M. Smith, N. Zhao, V. Bulovic, M. Bawendi and S. Gradecak, *Nano Lett.*, 2011, **11**, 3998–4002.
24 Y. J. Huang, W. C. Lo, S. W. Liu, C. H. Cheng, C. T. Chen and J. K. Wang, *Sol. Energy Mater. Sol. Cells*, 2013, **116**, 153–170.
25 G. E. Jabbour and D. Doderer, *Nat. Photonics*, 2010, **4**, 604–605.
26 K. Kumari, S. Chand, V. D. Vankar and V. Kumar, *Appl. Phys. Lett.*, 2009, **94**, 213503-1–213503-3.
27 E. Couderc, N. Bruyant, A. Fiore, F. Chandezon, D. Djurado, P. Reiss and J. F. Vincent, *Appl. Phys. Lett.*, 2012, **101**, 133301-1–133301-4.
28 L. Martinez, A. Stavrinadis, S. Higuchi, S. L. Diedenhofen, M. Bernechea, K. Tajima and G. Konstantatos, *Phys. Chem. Chem. Phys.*, 2013, **15**, 5482–5487.
29 C. H. Chang, T. K. Huang, Y. T. Lin, Y. Y. Lin, C. W. Chen, T. H. Chu and W. F. Su, *J. Mater. Chem.*, 2008, **18**, 2201–2207.

30 S. S. Williams, M. J. Hampton, V. Gowrishankar, I. K. Ding, J. L. Templeton, E. T. Samulski, J. M. DeSimone and M. D. McGehee, *Chem. Mater*., 2008, **20**, 5229−5229.
31 Z. Sun, J. Li, C. Liu, S. Yang and F. Yan, *Adv. Mater*., 2011, **23**, 3648−3652.
32 S. S. Li, C. P. Chang, C. C. Lin, Y. Y. Lin, C. H. Chang, J. R. Yang, M. W. Chu and C. W. Chen, *J. Am. Chem. Soc*., 2011, **133**, 11614−11620.
33 S. D. Oosterhout, M. M. Wienk, S. S. van Bavel, R. Thiedmann, L. J. A. Koster, J. Gilot, J. Loos, V. Schmidt and R. A. J. Janssen, *Nat. Mater*., 2009, **8**, 818−824.
34 A. J. Moule, L. Chang, C. Thambidurai, R. Vidu and P. Stroeve, *J. Mater. Chem*., 2012, **22**, 2351−2368.
35 A. L. Briseno, T. W. Holcombe, A. I. Boukai, E. C. Garnett, S. W. Shelton, J. J. M. Frechet and P. Yang, *Nano Lett.*, 2010, **10**, 334−340.
36 W. J. E. Beek, M. M. Wienk and R. A. J. Janssen, *Adv. Funct. Mater*., 2006, **16**, 1112−1116.
37 S. D. Oosterhout, L. J. A. Koster, S. S. van Bavel, J. Loos, O. Stenzel, R. Thiedmann, V. Schmidt, B. Campo, T. J. Cleij, L. Lutzen, D. Vanderzande, M. M. Wienk and R. A. J. Janssen, *Adv. Energy Mater.*, 2011, **1**, 90−96.
38 H. C. Liao, C. S. Tsao, T. H. Lin, M. H. Jao, C. M. Chuang, S. Y. Chang, Y. C. Huang, Y. T. Shao, C. Y. Chen, C. J. Su, et al. *ACS Nano*, 2012, **6**, 1657−1666.
39 A. Lefrancois, B. Luszczynska, B. Pepin-Donat, C. Lombard, B. Bouthinon, J. M. Verilhac, M. Gromova, J. Faure-Vincent, S. Pouget, F. Chandezon, et al. *Sci. Rep*., 2014, **5**, 7768-1−7768-8.
40 M. C. Beard, K. P. Knutsen, P. Yu, J. M. Luther, Q. Song, W. K. Metzger, R. J. Ellingson and A. J. Nozik, *Nano Lett.*, 2007, **7**, 2506−2512.
41 T. Song, S. Lee, B. Sun, *J. Mater. Chem.*, 2012, **22**, 4216−4232.
42 F. Priolo, T. Gregorkiewicz, M. Galli and T. F. Krauss, *Nat. Nanotechnol.*, 2014, **9**, 19−32.
43 K. M. Coakley, B. S. Srinivasan, J. M. Ziebarth, C. Goh, Y. Liu and M. D. McGehee, *Adv. Funct. Mater.*, 2005, **15**, 1927−1932.
44 C. H. Kim, S. H. Cha, S. C. Kim, M. Song, J. Lee, W. S. Shin, S. J. Moon, J. H. Bahng, N. A. Kotov and S. H. Jin, *ACS Nano*, 2011, **5**, 3319−3325.
45 K. Saitow, *J. Phys. Chem. B*, 2005, **109**, 3731−3733.
46 K. Saitow, T. Yamamura and T. Minami, *J. Phys. Chem. C*, 2008, **112**, 18340−18349.
47 K. Saitow and T. Yamamura, *J. Phys. Chem. C*, 2009, **113**, 8465−8470.
48 S. Wei, T. Yamamura, D. Kajiya and K. Saitow, *J. Phys. Chem. C*, 2012, **116**, 3928−3934.
49 K. Saitow, In Laser Ablation in Liquids - Principles and Applications in the Preparation of Nanomaterials, Yang, G., Ed., Pan Stanford publishing: Singapore, 2011, Chapter 12.
50 S. Wei and K. Saitow, *Rev. Sci. Instrum.*, 2012, **83**, 073110-1−073110-8.
51 K. Saitow, Y. Okamoto and Y. F. Yano, *J. Phys. Chem. C*, 2012, **116**, 17252−17258.
52 T. Kitasako and K. Saitow, *Appl. Phys. Lett.*, 2013, **103**, 151912-1−151912-5.
53 D. Kajiya, S. Ozawa, T. Koganezawa and K. Saitow, *J. Phys. Chem. C*, 2015, DOI: 10.1021/jp510675r.
54 The photocurrent $I(t)$ is obtained from the voltage $V_{TOF}(t)$ of the TOF signal using the relation of $I(t) = V_{TOF}(t)/R$, where R is the load resistance and t is the time.
55 H. Scher and E. W. Montroll, *Phys. Rev. B*, 1975, **12**, 2455−2477.
56 A. J. Mozer, N. S. Sariciftci, A. Pivrikas, R. Osterbacka, G. Juska, L. Brassat and H. Bassler, *Phys. Rev. B*, 2005, **71**, 035214-1−035214-9.
57 Standard deviations ($\pm\sigma$) are obtained from 5 times measurements, all of which were conducted under the same experimental conditions.
58 The magnitude of mobility is dependent on the electric field E, the phenomenon of which has been frequently observed in disordered structures such as organic polymers, according to the results in Refs. 56 and 59. To compare the mobilities of the pristine and hybrid films, those measured at $E^{1/2}$ = 150 $V^{1/2}/cm^{1/2}$ were used as typical values.
59 A. J. Mozer and N. S. Sariciftci, *Chem. Phys. Lett.*, 2004, **389**, 438−442.
60 S. A. Choulis, Y. Kim, J. Nelson, D. D. C. Bradley, M. Giles, M. Shkunov and I. McCulloch, *Appl. Phys. Lett*., 2004, **85**, 3890−3892.
61 J. A. Merlo and C. D. Frisbie, *J. Phys. Chem. B*, 2004, **108**, 19169−19179.
62 S. Hugger, R. Thomann, T. Heinzel and T. Thurn-Albrecht, *Colloid Polym. Sci.*, 2004, **282**, 932−938.
63 M. Chang, J. Lee, N. Kleinhenz, B. Fu and E. Reichmanis, *Adv. Funct. Mater.*, 2014, **24**, 4457−4465.
64 G. Xiao, Y. Guo, Y. Lin, X. Ma, Z. Su and Q. Wang, *Phys. Chem. Chem. Phys*., 2012, **14**, 16286−16293.
65 Y. Kim, S. Cook, S. M. Tuladhar, S. A. Choulis, J. Nelson, J. R. Durrant, D. D. C. Bradley, M. Giles, I. McCulloch, C. Ha and M. Ree, *Nat. Mater.*, 2006, **5**, 197−203.
66 J. Clark, C. Silva, R. H. Friend and F. C. Spano, *Phys. Rev. Lett.*, 2007, **98**, 206406-1−206406-4.
67 Y. Gao and J. K. Grey, *J. Am. Chem. Soc.*, 2009, **131**, 9654−9662.
68 G. Janssen, A. Aguirre, E. Goovaerts, P. Vanlaeke, J. Poortmans and J. Manca, *Eur. Phys. J. Appl. Phys*., 2007, **37**, 287−290.
69 W. C. Tsoi, D. T. James, J. S. Kim, P. G. Nicholson, C. E. Murphy, D. D. C. Bradley, J. Nelson and J. Kim, *J. Am. Chem. Soc*., 2011, **133**, 9834−9843.
70 S. Wood, J. S. Kim, D. T. James, W. C. Tsoi, C. E. Murphy and J. S. Kim, *J. Chem. Phys.*, 2013, **139**, 064901-1−064901-9.
71 The low-frequency component in the Raman band has been attributed to P3HT with a planar backbone structure, based on theoretical investigation of the vibrational frequency of the C=C stretching mode in Refs 69 and 70. The increase in the planarity of the P3HT backbone is attributed to an increase in the degree of aggregation, according to Ref. 67. Thus, the low frequency component is assigned to the C=C stretching mode of aggregated P3HT species, according to Ref. 67.
72 C. Y. Liu, Z. C. Holman and U. R. Kortshagen, *Nano Lett*., 2009, **9**, 449−452.
73 D. Li and R. B. Kaner, *J. Mater. Chem.*, 2007, **17**, 2279−2282.
74 D. Li and R. B. Kaner, *J. Am. Chem. Soc.*, 2006, **128**, 968−975.
75 Both previous and present studies used P3HT sourced from the same company (see Table S2†).
76 R. J. Kline, M. D. McGehee, E. N. Kadnikova, J. Liu, J. M. J. Fréchet and M. F. Toney, *Macromolecules*, 2005, **38**, 3312−3319.
77 J.-M. Verilhac, G. LeBlevennec, D. Djurado, F. Rieutord, M. Chouiki, J.-P. Travers and A. Pron, *Synth. Metals*, 2006, **156**, 815−823.
78 B. S.-Hansberg, M. Sanyal, M. F. G. Klein, M. Pfaff, N. Schnabel, S. Jaiser, A. Vorobiev, E. Muller, A. Colsmann, P. Scharfer, D. Gerthsen, U. Lemmer, E. Barrena and W. Schabel, *ACS nano*, 2011, **11**, 8579−8590.
79 T. S. Ripolles, A. Guerrero, and G. Garcia-Belmonte, *Appl. Phys. Lett.*, 2013, **103**, 243306-1−243306-5.
80 M. Brinkmann, *J. Polym. Sci., Part B: Polym. Phys*., 2011, **49**, 1218−1233.
81 K. U. Kao, S. C. Lo, H. L. Chen, J. H. Chen and S. Chen, *J. Phys. Chem. B*, 2014, **118**, 14510−14518.

82 To quantify the Si-NCs structure, we conducted the element analysis of Si-NCs. The result indicates the thickness of passivation layer is estimated as 0.27 nm (Fig. S9†) and the energy band diagrams reported in refs. 83 and 84 show no barrier for electron transfer from P3HT to Si (Fig. S10†).
83 F. Zhang, B. Sun, T. Song, X. Zhu and S. Lee, *Chem. Mater.* 2011, **23**, 2084–2090.
84 L. He, C. Jiang, H. Wang, D. Lai and Rusli, *Appl. Phys. lett*. 2012, **100**, 073503.
85 J. C. Dobrowolski, S. Ostrowski, R. Kołos and M. H. Jamroz, *Vib. Spectrosc.*, 2008, **48**, 82–91.
86 D. H. Kim, Y. Jang, Y. D. Park and K. Cho, *Macromolecules*, 2006, **39**, 5843–5847.
87 D. H. Kim, Y. D. Park, Y. Jang, H. Yang, Y. H. Kim, J. I. Han, D. G. Moon, S. Park, T. Chang, C. Chang, M. Joo, C. Y. Ryu and K. Cho, *Adv. Funct, Mater.*, 2005, **15**, 77–82.

Table of contents entry

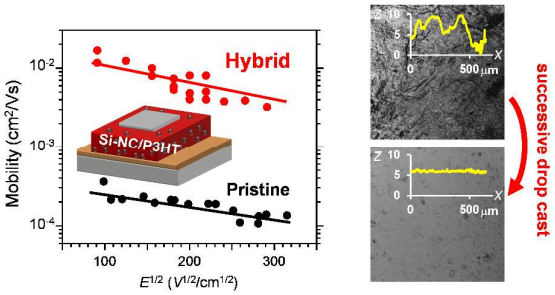

Hybrid Si-NC/P3HT film with good morphology and smooth surface is fabricated using a novel successive drop casting method.